Hindawi
Shock and Vibration
Volume 2024, Article ID 5676776, 9 pages
https://doi.org/10.1155/2024/5676776

Research Article

Simulation of Vortex-Induced Vibration for a Cylinder with Different Rounded Corners under Re = 150

Maofeng Gong,[1] Ruijia Jin,[2] Mingming Liu,[3] and Jianmin Qin[4,5]

[1]*Shandong Academy of Innovation and Development, Jinan 250101, China*
[2]*Tianjin Research Institute for Water Transport Engineering, MOT, Tianjin, China*
[3]*School of Architecture and Engineering, Liaocheng University, Liaocheng 252000, China*
[4]*Key Laboratory for Prediction & Control on Complicated Structure System of the Education Department of Liaoning Province, Dalian University, Dalian 116622, China*
[5]*College of Civil Engineering and Architecture, Dalian University, Dalian 116622, China*

Correspondence should be addressed to Jianmin Qin; qinjianmin@dlu.edu.cn

Received 28 November 2023; Revised 15 February 2024; Accepted 27 February 2024; Published 20 March 2024

Academic Editor: Traian Mazilu

A comprehensive 2D numerical model was conscientiously developed to investigate the vortex-induced vibration phenomena in a cylindrical structure with rounded corners. The Navier-Stokes equation was adeptly solved under the specific condition of a Reynolds number (Re) of 150. The investigation reveals intricate details of the phenomena. The study aimed to systematically analyze the interaction between drag and lift force coefficients, cylinder vibration amplitude, and the patterns of vortex shedding modes under various conditions. This study systematically altered the radius of the cylinder's rounded corners to evaluate their effects on both structural and hydrodynamic responses. This variation was crucial in comprehending how slight alterations in the cylinder's geometry impact significant changes in the flow dynamics and correlated vibration behavior. The model's numerical results revealed the significant impact of the curved edge ratio on both the hydrodynamic forces acting on the cylinder and its vibration response. The variation in edge curvature resulted in changes in drag and lift coefficients, leading to a significant impact on the amplitude of vibration. This elucidates the crucial role of geometric design in controlling and optimizing the structural behavior of cylindrical structures under fluid flow conditions.

1. Introduction

As water flows through a circular cylinder, a fluid dynamic phenomenon occurs where alternating vortices, called shedding vortices, form in a rhythmic pattern behind the cylinder. These vortices are not just a characteristic of fluid flow but have substantial implications on the cylinder itself as they exert periodic lift forces in the cross-flow direction. This interaction between fluid flow and cylinder results in vortex-induced vibration (VIV), which refers to a particular oscillatory movement the cylinder experiences from these forces. The phenomenon of "lock-in" represents a crucial aspect of this event, as it arises when the frequency of vortex shedding converges with or becomes closely aligned to the natural frequency of the cylinder. Natural frequency is an inherent property of any object, defining the frequency at which it tends to vibrate when disturbed. Resonance occurs during lock-in, causing a significant amplification of the cylinder's vibrations. This amplified vibration is of significant interest in various fields, ranging from engineering to environmental studies, as it significantly affects the structural integrity and behavior of cylindrical objects in fluid flows, such as pipelines, cables, and marine structures. It is essential to comprehend and predict VIV and lock-in conditions for designing structures that can withstand or evade these potentially destructive vibrations.

In the past few decades, the problem of vortex-induced vibration has attracted much attention from scholars all over the word. Feng [1] studied the frequency of the excitation force, the dimensionless amplitude, and the phase

difference between the cylindrical vibration displacement and the lift coefficient with respect to the reduced velocity in a wind tunnel for a D-shaped cylinder with mass ratio $m^* = 248$ and damping ratio $\xi = 0.00103$, and only cross-flow flow motion was allowed to occur. Khalak and Williamson [2] named the two branches of the displacement response found by Feng [1] as the initial branch and the lower branch, respectively. For the lower $m^*\xi$ case, three branches of the displacement response are found, namely, the initial branch, the upper branch, and the lower branch. In addition, the initial branch of the displacement response corresponds to the 2S vortex shedding mode and the lower branch to the 2P mode. Morse and Williamson [3] identified a new vortex-shedding mode "$2P_0$" through visualisation techniques. Lee and Lee [4] used numerical simulations to determine the Reynolds number Re = 200, different damping parameters $S_g S_g = 8\pi 2 S_t^2 \mathrm{a} M^*$, where $S_t = f_s D/U_\infty$ is the Strouhal number and $M^* = m/\rho D^2$ is the mass ratio), and the mass ratio of the cylinder when both inline and cross-flow motions are allowed to occur. Prasanth and Mittal [5] investigated numerically the vortex vibration of a cylinder with a mass ratio M^* of 10.0 at low Reynolds number ($60 < \mathrm{Re} < 200$) by means of a finite element method and found that the response of the cross-flow displacement can reach $0.6D$. The response of the cross-flow displacement also has two branches, the initial branch and the lower branch, and the initial branch corresponds to the vortex shedding mode of 2S and the lower branch corresponds to the vortex shedding mode of C. There have also been many fruitful studies on cylindrical vortex excitation vibration problems [6–14].

To summarize, many scholars have studied the flow-induced vibration problems of cylindrical or square cylinder. However, rounded corners are commonly applied to square cylinders in engineering applications, such as tension leg platforms in offshore engineering. There have been fewer studies on the flow-induced vibration of square cylinder with rounded corners. This study aims to investigate the effect of rounded corner on flow-induced vibration.

Due to the current lack of computational power in numerical analysis of 3D fluid-solid interaction turbulence, the Navier-Stokes equations of 2D incompressible viscous fluid are being solved using the upwind finite element numerical method. In addition, the arbitrary Lagrange–Euler (ALE) dynamic mesh method is being employed. To study the vortex-induced vibration of a cylinder, a computational program and numerical model have been developed. Re = 150 is taken as the representative for studying the vortex-induced vibration of a cylinder with rounded corners.

2. Numerical Model

2.1. Governing Equations. The governing equations for the motion of two-dimensional incompressible viscous Newtonian fluids are continuity equation and Navier-Stokes equations, which can be expressed in the following dimensionless form:

$$\frac{\partial u_i}{\partial x_i} = 0,$$
$$\frac{\partial u_i}{\partial t} + c_j \frac{\partial u_i}{\partial x_j} = -\frac{\partial p}{\partial x_i} + \frac{1}{\mathrm{Re}} \frac{\partial}{\partial x_j}\left(\frac{\partial u_i}{\partial x_j}\right), \tag{1}$$

where x_i denote the Cartesian coordinates ($i = 1$ and 2 in the two-dimensional case, corresponding to the x and y directions, respectively), u_i is the velocity in x_i direction, p is the pressure, $\mathrm{Re} = UD/\upsilon$ is the Reynolds number, U is the uniform incoming flow velocity, D is the diameter of the circular cylinder, υ is the kinematic viscosity coefficient of the fluid, and c_j is the convective velocity, which can be expressed as follows:

$$c_j = u_j - u_j^m, \tag{2}$$

where u_j^m denotes the motion velocity of the grid in j direction under the ALE reference coordinate system.

When the flow field and pressure field are obtained, the fluid force on the circular cylinder can be obtained by surface integration of the pressure and viscous shear force on the surface of the circular cylinder. Then, the nondimensional drag force coefficient C_D and the lift coefficient C_L can be written as

$$C_D = -\int_0^{2\pi} p\cos\theta d\theta - \frac{1}{\mathrm{Re}}\int_0^{2\pi}\left(\frac{\partial v}{\partial x} - \frac{\partial u}{\partial y}\right)\sin\theta d\theta,$$
$$C_L = -\int_0^{2\pi} p\sin\theta d\theta + \frac{1}{\mathrm{Re}}\int_0^{2\pi}\left(\frac{\partial v}{\partial x} - \frac{\partial u}{\partial y}\right)\cos\theta d\theta, \tag{3}$$

where θ is the angle between the line between the point on the circular cylinder and the center of the circular cylinder and the forward direction of the x axis.

The average value of the drag force coefficient can be expressed as

$$C_D^M = \int_{t_1}^{t_2} \frac{C_D(t)\mathrm{d}t}{\Delta T}, \tag{4}$$

where $\Delta T = t_2 - t_1$ is the time length of the drag force stabilization section.

The root mean square value of the drag force coefficient C_D^{RMS} can be expressed as

$$C_D^{\mathrm{RMS}} = \left[\int_{t_1}^{t_2} \frac{\left(C_D(t) - C_D^M\right)^2 dt}{\Delta T}\right]^{1/2}. \tag{5}$$

The maximum lift coefficient is

$$C_L^A = C_L^{\mathrm{MAX}} - C_L^M. \tag{6}$$

2.2. Equation of Motion for the Cylinder. The vortex-induced vibration problem of a cylinder can usually be treated to a mass-damp-spring vibration system. Under the constraints of fluid force, damping force, and spring, a dimensional equation of motion for the circular cylinder can be expressed as

$$m\ddot{X}_i + c\dot{X}_i + kX_i = 0.5\rho DU^2 C_i, \tag{7}$$

where, X_i, $\dot{X}_i$, and $\ddot{X}_i$ are the displacement, velocity, and acceleration in the direction of x, respectively. m, C, and k are the mass, structural damping, and spring stiffness of the circular cylinder, ρ is the density of the fluid, and C_i denotes the fluid force coefficient in the direction i. We further use the dimensionless relation $\ddot{x}_i = \ddot{X}_i D/U^2$, $\dot{x}_i = \dot{X}_i/U$, $x_i = X_i/D$, and $f_n = F_n D/U$; F_n is the natural vibration frequency of the system and the structural dynamics relation $k/m = (2\pi F_n)^2$, $c/m = 4\pi\xi F_n$. And, considering the definitions of the damping ratio and mass ratio ($\xi = c/4\pi m F_n$ and $m^* = 4m/\pi\rho D^2$), the dimensionless cylinder vibration equation can be obtained as follows:

$$\begin{aligned} \ddot{x} + 4\pi\xi f_n \dot{x} + (2\pi f_n)^2 x &= \frac{2C_D}{\pi m^*}, \\ \ddot{y} + 4\pi\xi f_n \dot{y} + (2\pi f_n)^2 y &= \frac{2C_L}{\pi m^*}. \end{aligned} \tag{8}$$

When the displacement of the cylinder is determined, the grid is updated by the differential mesh transformation method. Then, the new grid coordinates and grid velocity are obtained, which are used to solve the flow field at the next time step.

2.3. Computing Model and Boundary Conditions. The calculation model of this paper is shown in Figure 1. The center of the cylinder is located at the origin of coordinates (0.0, 0.0). In order to eliminate the influence of truncation boundary, the length of the calculation domain in this paper is $55D$ in the up-flow direction and $50D$ in the cross-flow direction. The dimensionless velocities $u = 1.0$ and $v = 0.0$ are specified at the entrance. Symmetric boundary conditions u are used on the side walls $\partial u/\partial y = 0$, $v = 0$. The velocity boundary condition at the exit is $\partial u_i/\partial t + c\partial u_i/\partial x_i = 0$, where c is the local average flow velocity; $u = \mathrm{d}x/\mathrm{d}t$ and $v = \mathrm{d}y/\mathrm{d}t$ are applied on the cylinder surface. In the calculation, the relative pressure $p = 0$ is specified at the outlet and $\partial p/\partial \mathbf{n} = 0$ is used at the other boundaries, where $\mathbf{n}$ is the external normal unit vector indicating the fluid domain. At the initial time, the velocity and pressure distributions in the flow field are set to zero, that is, the initial conditions satisfy the continuum equation.

In the simulation, the cylinder is allowed vibration only in y direction. The mass ratio is set to be 2.0 and the damping factor is 0.007. The Reynolds number is set to be 150 in this study.

The mesh configuration surrounding the cylinder is illustrated in Figure 2. This figure clearly demonstrates that the mesh density is significantly higher in the vicinity of the cylinder. This dense meshing is critical for capturing the intricate flow dynamics effects near the cylinder's surface with higher precision. As one moves away from the cylinder, the mesh becomes progressively sparser. This gradation in mesh density is strategically designed to optimize computational resources. By reducing the number of mesh elements in regions of lesser interest, where flow or thermal gradients are expected to be less intense, and computational time can be significantly reduced. This approach strikes a balance between computational efficiency and the accuracy of the simulation results. Furthermore, a noteworthy aspect observed from the figure is the retention of high-quality mesh even after the cylinder undergoes motion. This indicates the robustness of the mesh design, ensuring that it can adapt to changes in the physical configuration without losing its integrity. Such a feature is crucial in dynamic simulations where the geometry of interest is subject to movement or deformation. The mesh's ability to maintain its quality under such conditions is indicative of advanced meshing algorithms and thoughtful design, ensuring that the accuracy of the computational model is not compromised over the course of the simulation.

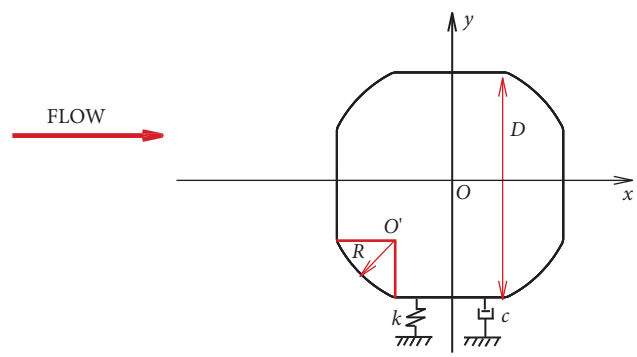

Figure 1: Sketch definition of the computational domain.

The numerical model used in this study is consistent with the numerical model used by Liu et al. [10–12], and the validation of the correctness of the model can be found in the paper by Liu et al. [10–12], which will not be discussed here.

3. Results and Discussion

3.1. Forces on the Cylinder. The drag force coefficients of a cylinder over time are analyzed for various reduced velocities, represented by the equation $\mathrm{Vr} = U/f\,D$, where U denotes the inlet velocity, f is the natural frequency of the cylinder, and D is the cylinder's diameter, at $R = 0.25$, as illustrated in Figure 3. The graph reveals a consistent pattern in how the drag force coefficient changes with time. For lower reduced velocities, specifically at ($\mathrm{Vr} = 2.0$), as well as higher reduced velocities, such as $\mathrm{Vr} = 6.0$, the drag force coefficient displays relatively small fluctuations in amplitude. Contrastingly, at intermediate reduced velocities, particularly at $\mathrm{Vr} = 4.0$ and $\mathrm{Vr} = 5.0$, there is a noticeable increase in the vibration amplitude of the drag force coefficient. Interestingly, at a reduced velocity of $\mathrm{Vr} = 4.0$, the behavior of the drag force coefficient diverges from the typical sinusoidal pattern observed at other velocities. This deviation from sinusoidal variation implies a complex interaction between the cylinder and the fluid flow at this specific reduced velocity, possibly indicating the onset of vortex-induced vibrations or other nonlinear dynamic phenomena.

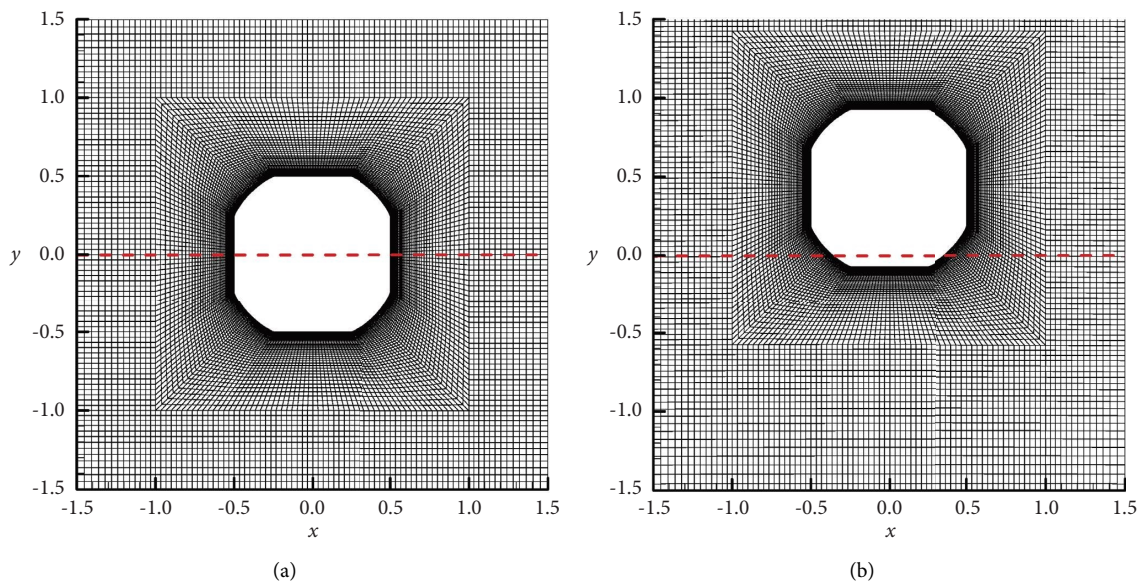

Figure 2: Meshes around the cylinder. (a) Initial meshes. (b) Meshes after motion.

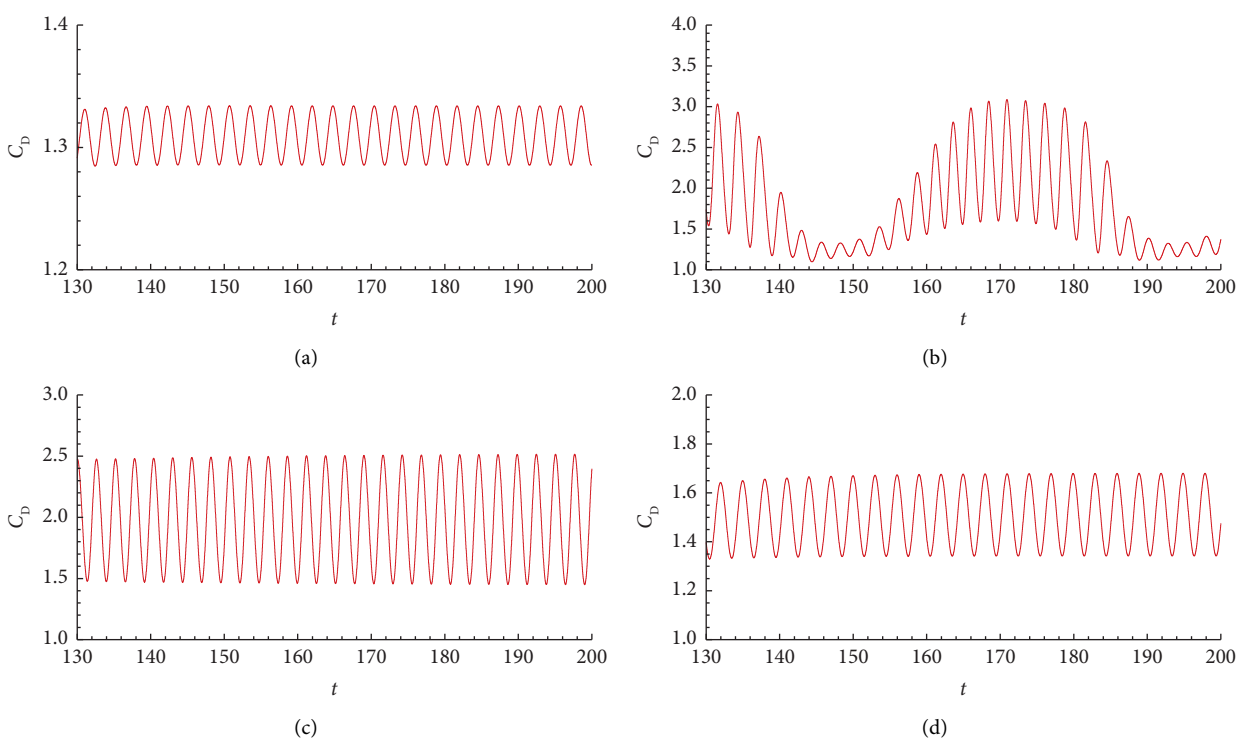

Figure 3: Drag force coefficients of the cylinder with time for different reduced velocities with $R/D = 0.25$. (a) Vr = 2.0. (b) Vr = 4.0. (c) Vr = 5.0. (d) Vr = 6.0.

Figure 4 depicts an in-depth analysis of the variation in the average drag force coefficient value concerning reduced velocity. This study is vital in comprehending the fluid dynamics surrounding objects of varying shapes and sizes. The chart displays a uniform pattern of variation across different R/D ratios, proving the universality of this behavior in fluid dynamics. The data can be segmented into three distinct regions based on the reduced velocity values. The first region, which corresponds to small reduced velocities, exhibits a minimal average value of the drag force coefficient.

As we move towards the middle region, we observe a significant rise in the average drag force coefficient value. This region holds great significance for engineering applications as it portrays high drag force on the cylinder, having a substantial impact on the stability and performance of diverse structures.

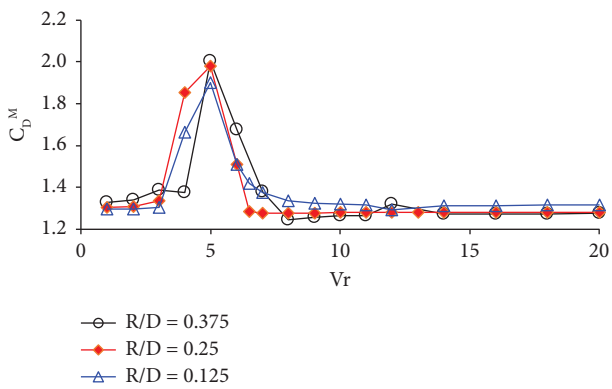

Figure 4: Dependence of C_D^M on reduced velocity.

On the contrary, the third region having large reduced velocities manifests a decline in the average drag force coefficient value, converging towards its initial lower levels.

Furthermore, the data presented in Figure 3 provide further evidence of this trend. The consistency between Figures 3 and 4 strengthens the validity of these observations and emphasizes their significance in hydrodynamics design.

Figure 5 depicts the lift coefficient time history lines for varying reduced velocity conditions, measured at a dimensionless cylinder radius to the diameter ratio (R/D) of 0.25. The graphical representation illustrates the dynamic behavior of the lift coefficient as it varies with time under different flow velocities, showcasing distinct patterns.

When analyzing the curves, an observable trend can be noted in the lift coefficient response when linked with different reduced velocities. It is worth mentioning that the cases with reduced velocities of 2.0 and 5.0 show a more predictable and coherent lift coefficient fluctuation pattern, with a clear and regular sinusoidal wave pattern. This pattern indicates a rhythmic and stable oscillation of the aerodynamic forces on the cylinder. The sinusoidal pattern of these fluctuations indicates that hydrodynamic forces operating on the cylinder in these flow conditions are stable, which may lead to a consistent response.

On the other hand, an investigation into the lift coefficient's time history at reduced velocities of 4.0 and 6.0 reveals a more erratic behavior pattern. The sinusoidal waves that suggest periodic force are substituted with intricate, nonperiodic variations. This difference is especially noticeable when focusing on the reduced velocity of 4.0, where the curves exhibit the most significant vibration amplitude in the lift coefficient. This significant amplitude indicates that the cylinder undergoes a pronounced fluctuation in hydrodynamic forces.

The root mean square (RMS) value of the lift coefficient varies with changes in the reduced velocity rate, as shown in Figure 6. This figure illustrates how the lift coefficient RMS value fluctuates with changes in the reduced velocity and reveals a consistent pattern across various diameter ratios (R/D). The graph in Figure 7 shows that across all the examined diameter ratios, there is an initial increase in the RMS value of the lift coefficient as the reduced velocity rises, with this trend observable uniformly for different R/D ratios. The increase continues steadily until it reaches a peak at a reduced velocity (Vr) of around 4.0. This peak denotes the maximum attainable value of lift coefficient RMS under the existing conditions. After the stated peak, there is an abrupt and drastic decrease in the RMS value of the lift coefficient. This reduction marks a considerable alternation in the hydrodynamic conduct of the object at this specific velocity. The sudden decline is potentially caused by diverse vortex shedding, which will be explicated in the upcoming sections. After the initial drop, the RMS value of the lift coefficient reaches a stable point and experiences little variation as the reduced velocity increases. This suggests that beyond a certain point, further increases in the reduced velocity have a diminishing impact on the RMS value of the lift coefficient.

3.2. Motion of the Cylinder. Figure 7 provides a comprehensive analysis of the time-dependent behavior of cylindrical vibration displacement. It shows that when the reduced velocity (Vr) is 2.0, the cylinder displays a regular vibration pattern. Remarkably, the amplitude of these vibrations consistently remains low, with a peak value less than 0.02. It implies that at lower velocities, the system retains a stable and minimal vibrational state. As the decreased velocity increases to 4.0, a noticeable alteration in the vibrational pattern happens. The loudness of the vibration displays a recurring conduct, fluctuating between amplifying and diminishing over time. This is important because it denotes a shift in the dynamic reaction of the cylinder as the velocity varies. The maximum amplitude observed at this velocity significantly increases, reaching approximately 0.6. Further increasing the reduced velocity to 5.0 leads to another shift in the system's vibrational characteristics. It returns to a pattern of vibration similar to that observed at the lower velocity of 2.0. Nevertheless, the maximum amplitude of vibration at this stage is notably lower than what is observed at Vr = 4.0. At a reduced velocity of 6.0, the trend persists with a further decrease in vibration amplitude.

The relationship between reduced velocity and vibration amplitude, as discussed, illustrates a crucial aspect of cylindrical structure dynamics. Figure 8 provides a detailed analysis of how the root mean square (RMS) value of cylindrical vibration displacement changes with reduced velocity, indicating this relationship. This figure is crucial in comprehending the dynamics at play. The figure reveals a consistent pattern in RMS value variation across varying diameter ratios (R/D) in cylindrical structures. This consistency implies a universal principle governing their vibration behavior, independent of their diameter ratios. Importantly, the diameter ratio (R/D) plays a crucial role in structural design as it impacts the stability of the structure. In addition, the data suggest that at both lower and higher levels of reduced velocity, the displacement RMS values are relatively smaller. The graphic clearly illustrates a direct correlation between the ratio of diameter (R/D) and the highest RMS value of displacement. As the diameter ratio increases, the maximum displacement RMS value steadily increases as well.

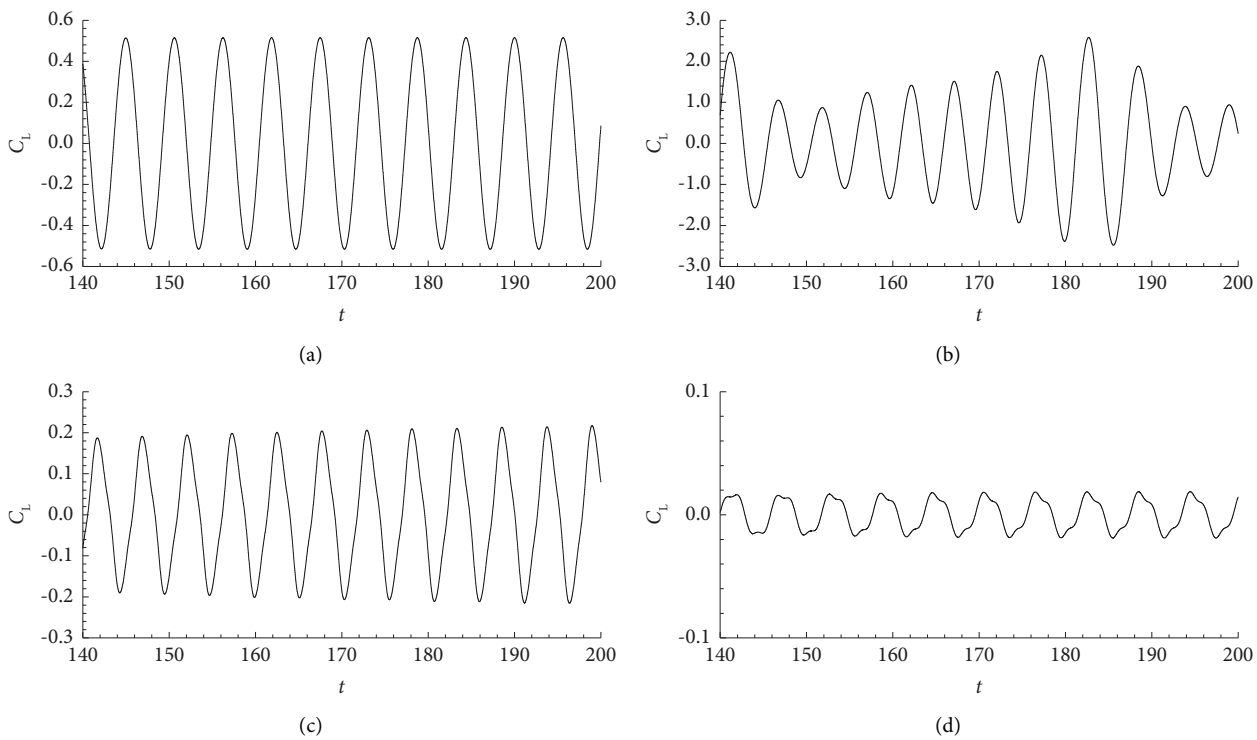

Figure 5: Lift force coefficients of the cylinder with time for different reduced velocities with $R/D = 0.25$. (a) Vr = 2.0. (b) Vr = 4.0. (c) Vr = 5.0. (d) Vr = 6.0.

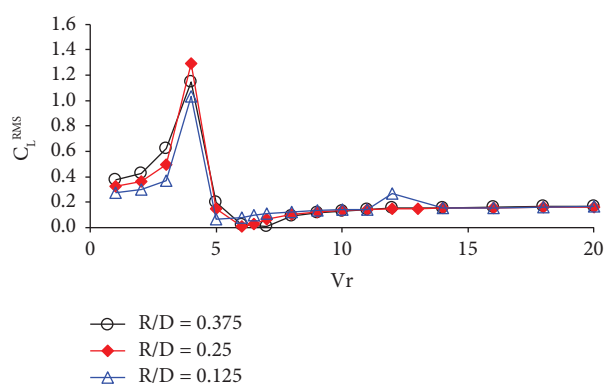

Figure 6: Dependence of C_L^{RMS} on reduced velocity.

3.3. Vortex Shedding Mode of the Cylinder. The analysis of the forces and vibrations of a cylinder at different reduced velocities highlights a complex interplay between fluid dynamics and the cylinder's structural response. This complexity is caused by the various patterns of wake vortex shedding, illustrated in Figure 9. The vortex distribution around the cylinder when the cylinder is at the maximum position for different reduced speeds is given in Figure 9.

At lower reduced velocities, like Vr = 2.0, and higher ones, such as Vr = 6.0, the wake vortices shed from the cylinder alternate. This phenomenon exemplifies the von Kármán vortex street, a recognized pattern in fluid dynamics where vortices are consistently shed from opposing sides of a bluff body. The uniformity of this shedding pattern at these speeds affects the forces applied to the cylinder and its consequential vibrational reaction.

However, a significant deviation is observed at a decreased velocity of Vr = 4.0. This discrepancy is characterized by the considerably shorter length of the wake vortices. This reduction in the vortex size signifies a more turbulent and energetic wake, leading to an increase in the forces exerting on the cylinder. Specifically, the higher pressure differential created by the shorter vortices leads to more pronounced vibrational displacements.

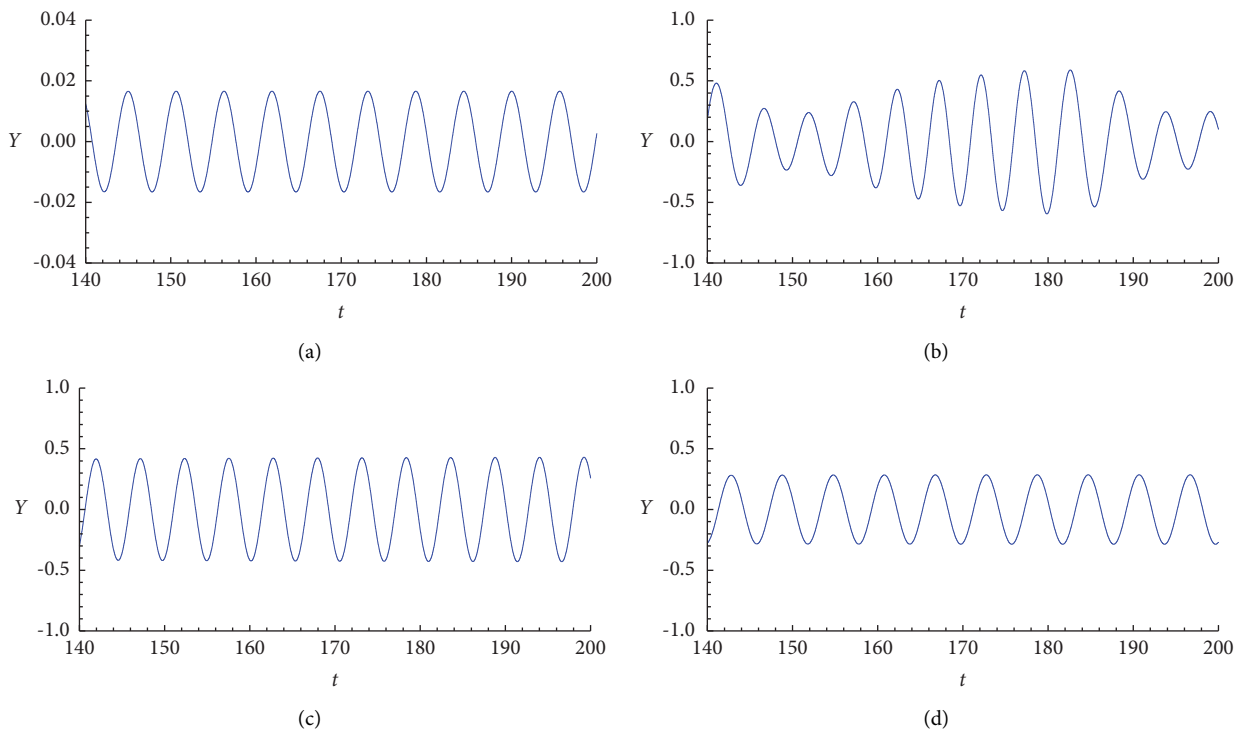

Figure 7: Motion of the cylinder with time for different reduced velocities with $R/D = 0.25$. (a) Vr = 2.0. (b) Vr = 4.0. (c) Vr = 5.0. (d) Vr = 6.0.

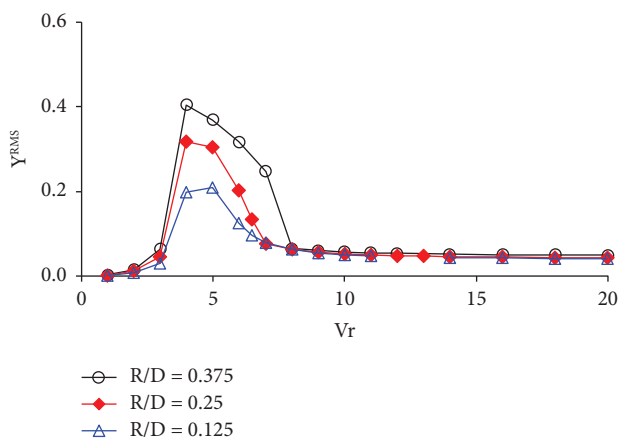

Figure 8: Dependence of Y^{RMS} on reduced velocity.

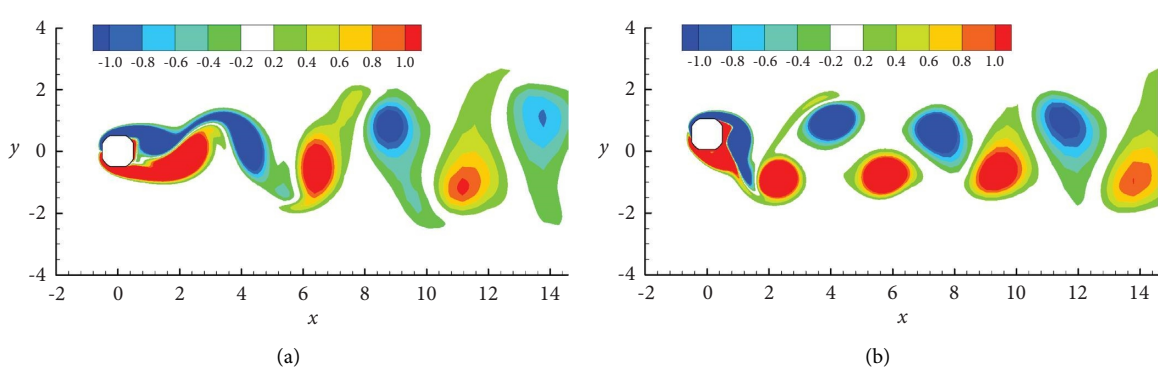

Figure 9: Continued.

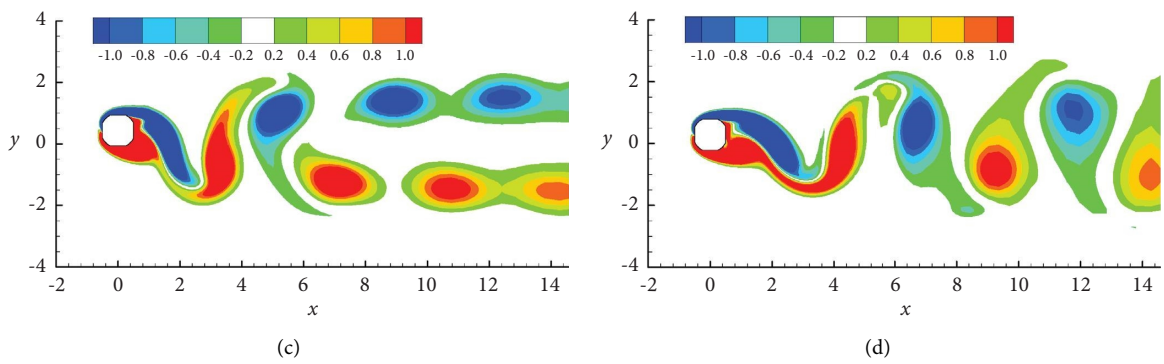

Figure 9: Vortex-shedding mode for different reduced velocities with $R/D = 0.25$. (a) Vr = 2.0. (b) Vr = 4.0. (c) Vr = 5.0. (d) Vr = 6.0.

In addition, when the velocity is increased, the wake vortices no longer align in a single row as observed at lower velocities. Instead, they exhibit a dual-row arrangement, suggesting a change in flow dynamics surrounding the cylinder, possibly due to modifications in the behavior of the boundary layer or flow separation points on the surface of the cylinder.

At Vr = 5.0, another distinct pattern emerges. Close to the cylinder, vortices arrange themselves linearly, suggesting a flow regime concurrent with lower velocities. However, as distance from the cylinder increases, vortices form in two rows, indicating intricate interplay between the cylinder's boundary layer and the wake region. The dual pattern at Vr = 5.0 proposes a transitional phase in the flow dynamics, where the features of both lower and higher reduced velocities manifest.

4. Conclusion

In this comprehensive study, a two-dimensional numerical model was implemented to investigate vortex-induced vibrations (VIVs) in a cylinder, with specific focus on variations in rounded corner geometries. The Navier-Stokes equations were solved within a defined parameter of Reynolds number (Re) set at 150 to simulate realistic fluid dynamics scenarios. The study systematically investigated the effects of altering the cylinder's diameter ratio (R/D) and reduced velocity on a range of critical factors. These factors encompassed the forces borne by the cylinder, the resulting oscillation amplitude, and the characteristic modes of vortex shedding, all of which play pivotal roles in comprehending the structure's dynamic response when immersed in fluid flow conditions. From the simulation and discussion, the following conclusions can be obtained in the present study scope.

(1) The trends of forces on the cylinder and displacements with the reduced velocity are the same for different diameter ratios (R/D).

(2) Large diameter ratios (R/D) lead to greater Y^{RMS}, but the mean drag force and RMS value of lift force are not much difference.

(3) At the same diameter ratio (R/D), different vortex-shedding modes result in different cylindrical forces and vibrational displacements at different reduced velocities.

Data Availability

The data used to support the findings of this study are included within the article.

Conflicts of Interest

The authors declare that they have no conflicts of interest.

Acknowledgments

This work was supported by the Natural Science Foundation of Sichuan Province of China (2023YFQ0111).

References

[1] C. C. Feng, *The Measurement of Vortex Induced Effects in Flow Past Stationary and Oscillating Circular and D-Section Cylinders*, University of British Columbia, Vancouver, Canada, 1968.

[2] A. Khalak and C. H. K. Williamson, "Motions, forces and mode transitions in vortex-induced vibrations at low mass-damping," *Journal of Fluids and Structures*, vol. 13, no. 7-8, pp. 813–851, 1999.

[3] T. L. Morse and C. H. K. Williamson, "Prediction of vortex-induced vibration response by employing controlled motion," *Journal of Fluid Mechanics*, vol. 634, pp. 5–39, 2009.

[4] M. Lee and S. Lee, "Vortex-induced vibrations of a circular cylinder at low Reynolds numbers," *KSME International Journal*, vol. 17, no. 11, pp. 1628–1637, 2003.

[5] T. K. Prasanth and S. Mittal, "vortex-induced vibrations of a circular cylinder at low Reynolds numbers," *Journal of Fluid Mechanics*, vol. 594, pp. 463–491, 2008.

[6] T. Guo-qiang, *A Study on Numerical and Experimental Investigation into Vortex-Induced Vibration of marine Risers*, Dalian University of Technology, Dalian, China, 2011.

[7] W. Chen, A. Ren, and G. Li, "The numerical study of two-degree-of freedom vortex-induced vibration of the downstream cylinder in tandem arrangement (In Chinese)," *Journal of Mechanics*, vol. 36, no. 6, pp. 732–738, 2004.

[8] Z. Kang and L. Jia, "An experiment investigation on viv trajectories of a two degree free vibration cylinder (In Chinese)," *Journal of Mechanics*, vol. 44, no. 6, pp. 970–980, 2012.

[9] Y. Bao, D. Zhou, and J. H. Tu, "Flow interference between a stationary cylinder and an elastically mounted cylinder arranged in proximity," *Journal of Fluids and Structures*, vol. 27, no. 8, pp. 1425–1446, 2011.

[10] M. M. Liu, X. Jin, L. Wang, F. Yang, and J. B. Tang, "Numerical investigation of local scour around a vibrating pipeline under steady currents," *Ocean Engineering*, vol. 221, Article ID 108546, 2021.

[11] M. M. Liu, R. J. Jin, and H. C. Wang, "Numerical investigation of vortex induced vibration of a circular cylinder for mass ratio less than 1.0," *Ocean Engineering*, vol. 251, Article ID 111130, 2022a.

[12] M. M. Liu, H. C. Wang, F. F. Shao, X. Jin, G. Q. Tang, and F. Yang, "Numerical investigation on vortex-induced vibration of an elastically mounted circular cylinder with multiple control rods at low Reynolds number," *Applied Ocean Research*, vol. 118, Article ID 102987, 2022b.

[13] X. Zhang, M. Hu, J. Cai, A. Babenko, E. Shiju, and Z. Xu, "Numerical simulation of vortex-induced transverse vibration of a cylinder with very low mass ratio," *Shock and Vibration*, vol. 2022, Article ID 3520982, 13 pages, 2022.

[14] M. Yu, X. Wang, J. Cai et al., "Analysis on flow-induced vibration of square cylinders with different vibration forms and the flow energy harvesting capacity," *Physics of Fluids*, vol. 35, no. 9, Article ID 095124, 2023.